Lithospheric and upper mantle stratifications beneath Tibet: New insights from Sp conversions

Gerard Wittlinger, V. Farra, Jérôme Vergne

Lithospheric and upper mantle stratifications beneath Tibet: New insights from Sp conversions

G. Wittlinger,[1] V. Farra,[2] and J. Vergne[3]

Received 8 July 2004; revised 20 August 2004; accepted 16 September 2004; published 15 October 2004.

[1] We assess the upper mantle structure under the Tibetan plateau from a S-to-P converted waves receiver functions study. Contrary to the Ps receiver functions blurred by multiples from Moho to 350 km depth, the Sp are better suited for imaging at these depths. The Moho is clearly recovered and often exhibits a complex and warped structure. The upper crust is marked by a significant low velocity zone in the southern part of the plateau, probably associated with partial melt, which vanishes north of the Bangong suture. In the upper mantle, between the Moho and the 660 km discontinuity, four stratification levels are identified. The strongest converter at a depth ranging between 120 to 180 km corresponds to the bottom of a low shear-wave velocity layer imaged by surface wave inversion. *INDEX TERMS:* 7203 Seismology: Body wave propagation; 7205 Seismology: Continental crust (1242); 7218 Seismology: Lithosphere and upper mantle. **Citation:** Wittlinger, G., V. Farra, and J. Vergne (2004), Lithospheric and upper mantle stratifications beneath Tibet: New insights from Sp conversions, *Geophys. Res. Lett.*, *31*, L19615, doi:10.1029/2004GL020955.

1. Introduction

[2] Seismic velocity discontinuities in the upper mantle reflect changes in composition, temperature or mantle fabric. These changes in turn may reflect processes acting within the lithosphere and upper mantle related to large-scale tectonics. The Tibetan plateau is the largest orogene due to continental collision. In most of the recent models describing the formation and evolution of the Tibetan plateau, the upper mantle plays a role as important as the crust. Since mountain building along the northern edge of Tibet does not follow oceanic closure as in the South, different styles of mantle deformation are expected. While along the southern edge of the plateau, the Indian mantle with perhaps some crust subduct beneath the Himalayas [*Nelson et al.*, 1996], Asian lithospheric mantle likely subducts southwards beneath the northern Plateau [*Tapponnier et al.*, 2001; *Kind et al.*, 2002; *Wittlinger et al.*, 2004]. Such processes produce tectonic stacking in the crust but what happens in the upper mantle remains unclear.

[3] Models that invoke time dependent localized shear between coherent lithospheric blocks to explain how different parts of Tibet rose since the onset of collision [*Tapponnier et al.*, 2001] predict sequential intracontinental subduction of Asian lithospheric mantle beneath Northern Tibet. Direct observations of such subductions [*Kosarev et al.*, 1999; *Kind et al.*, 2002; *Vergne et al.*, 2002; *Wittlinger et al.*, 2004; *Shi et al.*, 2004] however are scarce and often blurred since they use Ps receiver functions migrations that are ill adapted for imaging upper mantle structures because multiples interfere with direct conversions. To better image crust and upper mantle, we use here S-to-P converted waves to compute Sp receiver functions (Sp-RFs here after), which are free from multiples and sensitive to weak velocity jumps.

2. Data and Analysis Method

[4] Although P-wave receiver functions are efficient for imaging crustal structures or deep upper mantle discontinuities, for example the 410–660 km discontinuities [*Kosarev et al.*, 1999; *Kind et al.*, 2002; *Wittlinger et al.*, 2004], they are less useful for discontinuities lying between the Moho and 410 km depth. The principal drawback is that multiples of the Ps conversions at intra crustal layers and at the Moho (Ppps, Ppss+Psps, Psss) arrive in a time window similar to that of direct Ps conversions generated in this depth interval. Such multiples may be very strong compared to direct Ps conversions occurring below the Moho, making the identification of mantle interfaces questionable. For Sp receiver functions the situation is different since all primary Sp conversions are precursors of the direct S-wave and the corresponding multiples arrive later than the direct S-wave. For these reasons, Sp-RFs should be ideally suited to upper mantle structure imaging.

[5] The method for computing Sp-RFs is described by *Farra and Vinnik* [2000]. Here we apply a simplified method using a time-domain iterative deconvolution of the vertical component by the radial. The Sp-RFs are computed with a technique similar to the Ps-RFs, exchanging only the respective role of the P and Sv components. The Sv-wave source function is isolated on the radial component before applying the deconvolution process. For this study, we use data from the Passcal 1991/92 [*Owens et al.*, 1993] and the Indepth II [*Nelson et al.*, 1996] and III [*Zhao et al.*, 2001] experiments (Figure 1). Only the strongest earthquakes ($M \sim >6$) can be used and the range of epicentral distances is also narrower. The lower bound of usable epicentral distances for S-to-P conversion studies is near 40° in order to avoid large take-off angles and thus converting points that are located far from the station. The upper bound of usable epicentral distances is about 100° since S and SKS phases can be used. Nothing ensures that the converters are really flat over such a great lateral distance. We thus restrain the back azimuth range of the incoming rays, using earthquakes with eastern back azimuths giving conversion points at a fictitious 150 km deep converter in a strip ~100 km large (Figure 1, dark blue

[1]Ecole et Observatoire des Sciences de la Terre, Strasbourg, France.
[2]Département de Sismologie, Institut de Physique du Globe Paris, Paris, France.
[3]Laboratoire de Géologie, Ecole Normale Supérieure, Paris, France.

0094-8276/04/2004GL020955

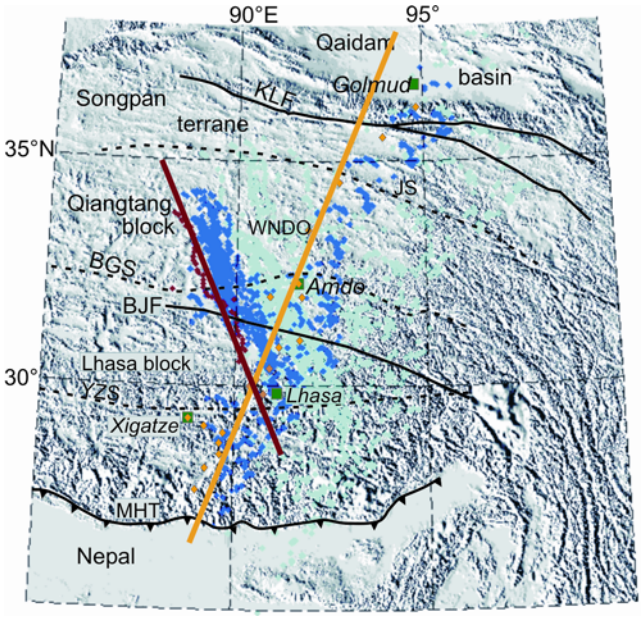

Figure 1. Locations of the stations used in this study on the topographic map of central Tibet. Red (resp. yellow) diamonds stand for stations used for western (resp. eastern) profile oriented N22°W (resp. N22°E). Orange diamonds are the stations common to the two profiles. Blue (resp. cyan) circles are the S-to-P wave conversion points at fictive 150 km (resp. 410 km) deep converters. Lines represent principal tectonic boundaries (MHT=Main Himalayan Thrust, YZS=Yarlung Zangpo suture, BJF=Bengco Jiali Fault, BGS = Bangong suture, JS=Jinsha suture and KLF=Kunlun faults).

points). The number of records at each station thus varies between 10 for some Indepth III stations to more than 50 for most of the Passcal stations.

[6] If the time and amplitude axes are reversed for the Sp-RFs, they look like the Ps-RFs (Figure 2). With this transformation on Sp-RFs, a downward positive (respectively negative) velocity variation produces positive (respectively negative) converted amplitude on both types of RFs. The Moho Ps and Sp conversions arriving (Figure 2) at about the same time (~10s after the P and S principal wave arrivals) best illustrate this. Both have positive amplitude, in agreement with the downward positive velocity gradient generally observed at the Moho interface. Similarly, the significant positive amplitude, clearly visible beyond the Moho conversion, ~23s after the S arrival on the Sp-RF and labelled "lithospheric interface" in Figure 2, corresponds to a downward positive velocity gradient. This conversion is hardly visible on the Ps-RF (Figure 2) since it falls in the time window of the crustal multiples.

3. Results

[7] We perform a common conversion point (CCP) migration of Sp-RFs. The Sp-RFs migration is done in a manner similar to that of the Ps-RFs migration, using ray tracing with an appropriate velocity model. Here we use the IASPEI model modified to take into account the ~70 km thick crust [*Kind et al.*, 2002; *Vergne et al.*, 2002], and the uppermost mantle layer between 70 and 150 km depth with the low velocity deduced from surface wave inversion [*Debayle and Sambridge*, 2004] and P*n* studies [*McNamara et al.*, 1997]. Two profiles at right angle to the main tectonic discontinuities are used for the migration sections and only stations located near the profiles are retained. The eastern profile, centered at 90.5°E 30°N is oriented N22°E, the western profile is centered at the same origin and oriented N22°W (Figure 1).

[8] For each profile, two sections are presented; the crustal section (depth range 0–125 km, Figures 3a and 3b) based on high frequency filtered data (0.5 to 0.1 Hz), and the upper mantle section (Figures 4a and 4b) based on low frequency filtered data (0.2 to 0.02 Hz). As the Sp-RFs are free of earth-surface multiples and even if very weak interlayer multiples may exist, all the significant positive or negative amplitudes are interpretable. The upper mantle migrated sections are a little blurred due to the large lateral extension of the deep conversion points.

[9] Along both profiles (Figure 3), the Moho interface is complex, discontinuous and warped, with depth ranging between ~50 km and ~90 km, consistent with previous Ps-RFs studies [*Kosarev et al.*, 1999; *Kind et al.*, 2002; *Vergne et al.*, 2002; *Galvé et al.*, 2002; *Shi et al.*, 2004]. Beneath the central Himalayas, two converters deepen northwards gradually and flatten at depths of 65 and 85 km forming a kind of "doublet" [cf. *Kind et al.*, 2002] south of the YZS. A similar structure is observed in the western most part of Tibet beneath the southern part of the Tibetan plateau [*Wittlinger et al.*, 2004]. The upper converter of the doublet might be the MHT (Main Himalayan Thrust) [*Zhao et al.*, 1993], and the deeper one the base of the under-thrust Indian crust [*Owens and Zandt*, 1997]. The Moho reaches its maximum depth (~90 km) in front of this downward toboggan. In the North, between the Jinsha suture and the Qaidam basin, the Moho rises in small steps from ~75 km to ~50 km depth similarly to what have been observed by *Vergne et al.* [2002]. The western profile

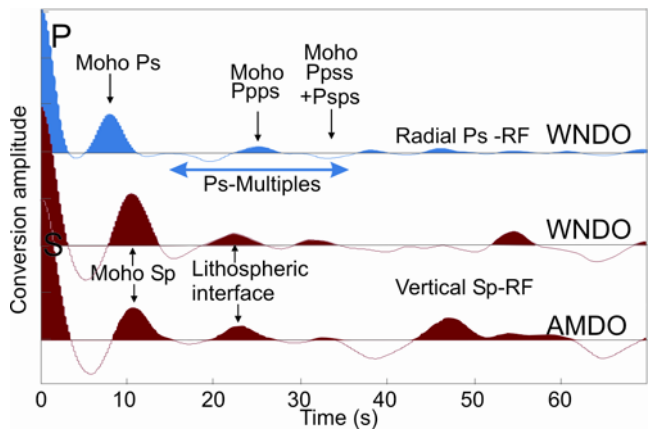

Figure 2. Stack of Ps (in blue, station WNDO) and Sp (in red, stations WNDO and AMDO) low frequency receiver functions corrected for move-out (8.4s/deg). Time and amplitude axis are reversed for Sp-RFs. The primary P and S waves are adjusted at same time zero and scaled at same amplitude. Arrows indicate Moho and lithospheric interfaces conversions.

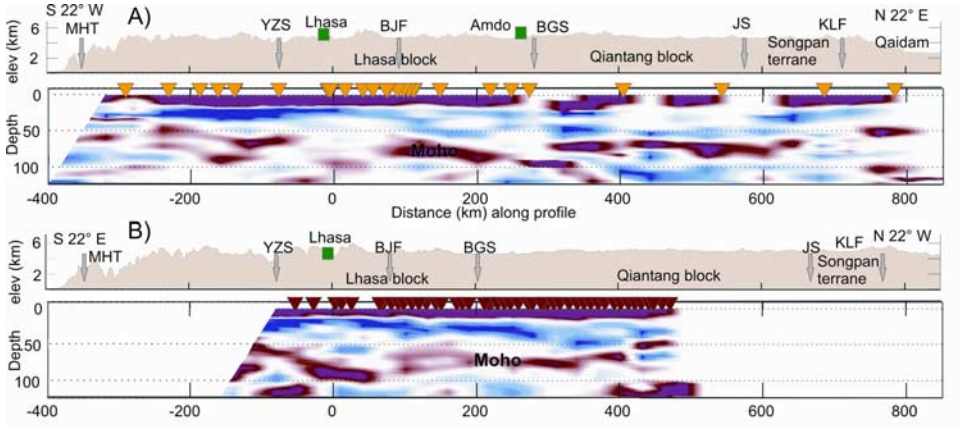

Figure 3. CCP migration restricted to the crust of high frequency Sp-RFs along (a) eastern profile (in yellow in Figure 1) and (b) along western profile (in red in Figure 1). Red (rep. blue) colour stands for positive (resp. negative) downward velocity gradients. Yellow and red triangles stand for stations projection on the profiles.

(Figure 3b) is compatible with these results and emphasizes the complexity of the lower crustal structure south of the BGS, as well as the particularly deep (∼90 km) Moho in the centre of the Lhasa block. On the same profile the amplitude of the Sp conversions at the Moho seems to be weak beneath the northern part of the Lhasa terrane. This relative weakness of the S-to-P conversions, in agreement with a similar weakness of the P-to-S conversions [*Shi et al.*, 2004] may indicate a more gradual change in the crust to mantle transition [*Meissner et al.*, 2004].

[10] Strikingly, Sp-RFs outline only negative downward velocity gradients in the crust. South of the YZS, all the way to the Himalayas, a well-defined negative velocity gradient (in blue) is observed in the upper crust. This zone becomes slimmer north of the YZS on the eastern profile and does not extend significantly north of the Bengco Jiali fault. On the western profile, the negative velocity gradient in the upper-middle crust remains well defined north of the BJF and BGS up to the Qiantang. This important negative velocity gradient in the upper crust may reflect presence of partial melt in a region where intrusive Miocene granites are frequent. On the eastern profile north of BJF this negative velocity gradient splits into two thinner layers and weakens, in agreement with the normal values (∼1.75) of the mean Vp/Vs deduced from Ps-RFs north of the BGS [*Vergne et al.*, 2002; *Kind et al.*, 2002]. The negative velocity gradients correlate fairly well with the electrical high conductivity zones usually associated with partial melt and aqueous fluids [*Wenbo et al.*, 2001].

[11] In the upper mantle, at depths ranging between ∼120 and ∼180 km a clear converter is seen between the YZS and the KLF. It appears to dip inwards reaching its maximum depth (∼180 km) beneath the BGS. Previous Ps-RFs studies have probably already shown evidence for such an interface, dubbed Indian (ILM) [*Kosarev et al.*, 1999] and Asian (ALM) lithospheric mantle [*Kind et al.*, 2002]. But the shape and the depth of this lithospheric interface as deduced from Sp-RFs, are significantly different from those inferred with Ps-RFs [*Kind et al.*, 2002] likely due to interference with Moho Ppps multiples. The 50 to 100 km thick layer overlying this interface coincides remarkably well in position and shape with the relatively low velocity layer obtained from surface wave inversion [*Debayle and Sambridge*, 2004], which is thickest (∼90 km) beneath BGS and thins gradually southward and northward.

[12] The Sp amplitude at the lithospheric interface is ∼25%–50% of the Sp amplitude at the Moho (Figure 2). This implies that the velocity contrasts at the Moho and at this interface are in the same proportion. At the Moho the S-wave velocity contrast is of about ∼+0.55 km/s [*Meissner et al.*, 2004]. Consequently at the base of this layer the S-wave velocity contrast may be locally as high as ∼+0.25 km/s. Lowering the velocity in the upper layer and increasing it in the underlying layer would be in keeping with the surface wave inversion results.

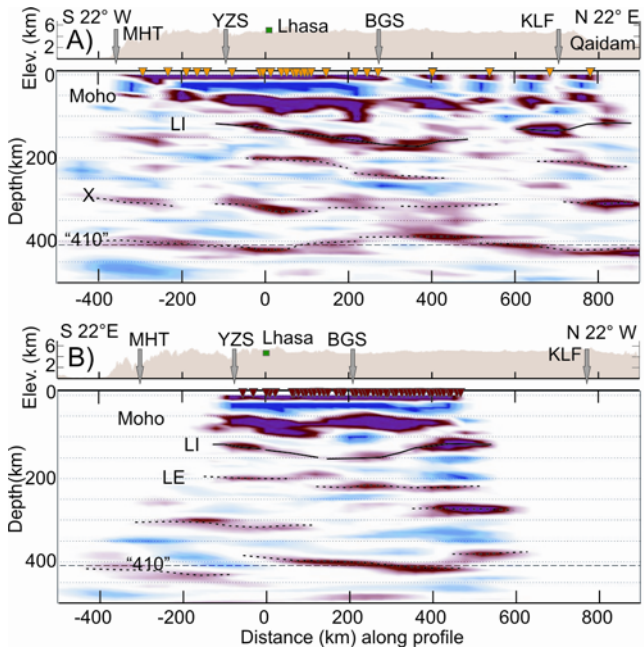

Figure 4. CCP migration of low frequency Sp RFs along eastern (a) and western (b) profiles as in Figure 3. Continuous line underlines lithospheric interface (LI) and broken lines other mantle stratifications at mean depths of 220 km (LE=Lehmann discontinuity), 310 km (X-discontinuity) and 410 km.

[13] The mid-Tibet lithospheric interface extends over hundreds of kilometres in the north-south direction and is well defined on both the eastern and western profiles giving evidence for a similarly broad east-west extent. There is also evidence, though still questionable because deduced from Ps conversions, for the existence of a similar interface beneath the western most part of Tibet [*Wittlinger et al.*, 2004]. The origin and nature of this lithospheric interface are puzzling. The mantle in the overlying layer may be mixed with lower crustal cuttings dragged down during sequential continental subduction in addition or alternatively to crustal material injected near major tectonic boundaries. Assuming that these materials are water rich, weak but pervasive melt could be generated, accounting for the lowered velocity. However, we do not observe strong negative downward velocity gradients in this layer that would imply significant partial melt. Alternatively, rapid change of the anisotropic parameters could also account for the strong Sp conversions at the base of this layer.

[14] The Sp conversions reveal other upper mantle discontinuities. The Lehmann discontinuity [*Lehmann*, 1961], supposed to have continental affinity is clear here especially on the Western profile (Figure 4b) at a depth ranging between 200 and 220 km. Around 310 km depth, one might recognize the so-called "X-discontinuity" [*Revenaugh and Sipkin*, 1994]. Sp conversions are not suited for imaging very deep interfaces like the "660 km" discontinuity due to the over critical angle of the incident S-waves. Even for the 410 km discontinuity, the migrated sections are blurred due to the very large lateral extension of the corresponding conversion points (see Figure 1, cyan circles) that are stacked in a unique section. Nevertheless the "410 km" discontinuity appears to undergo small local depth variations reflecting temperature and/or velocity variations.

4. Conclusion

[15] The Sp-RFs migration proves to be a powerful technique for crust and upper-mantle imaging complementary to the Ps-RFs migration in the depth range (60–400 km) where the later often fails because it is blurred by the multiples. The Sp-RFs yield sharp images of the lithospheric structure along sections crossing the central part of the Tibetan plateau from Nepal to Qaidam basin. Lithospheric structures observed along the northern and southern rims of the plateau are different, reflecting different modes of accommodation of convergence between India and Asia. North of the Himalayas, the north dipping Sp converters observed may reflect northward underthrusting of Indian crust beneath the MHT. In the central part of the plateau, the Sp-RFs images of the lower crust cleared of the multiples yield a particularly complex geometry of the crust-mantle transition making identification of Moho ambiguous at places.

[16] The specific contribution of the Sp converted waves lies in the unquestionable and clear image of a strong downward velocity increase located at the base of the lithosphere that deepens inwards from 120 to 180 km. The exact nature and origin of this interface and of the overlying layer remain puzzling. The nature of this layer and its role in Tibet structure and evolution critically depend on whether its velocity is significantly lower than normal or not. This role might include eastward displacement of lithospheric material that could contribute to create the anisotropic fabric observed beneath Tibet.

[17] **Acknowledgments.** This work was supported by program IT of INSU (Institut National des Sciences de l'Univers, France). Thanks also to Paul Tapponnier and Georges Poupinet for their help and to two anonymous reviewers for their constructive criticisms.

References

Debayle, E., and M. Sambridge (2004), Inversion of massive surface wave data sets: Model construction and resolution assessment, *J. Geophys. Res.*, *109*, B02316, doi:10.1029/2003JB002652.

Farra, V., and L. Vinnik (2000), Upper mantle stratification by *P* and *S* receiver functions, *Geophys. J. Int.*, *141*, 699–712.

Galvé, A., et al. (2002), Complex images of the Moho and variation of Vp/Vs across the Himalaya and South Tibet, from a joint receiver-function and wide-angle reflection approach, *Geophys. Res. Lett.*, *29*(24), 2182, doi:10.1029/2002GL015611.

Kind, R., et al. (2002), Seismic images of crust and upper mantle beneath Tibet: Evidence for Eurasian plate subduction, *Science*, *298*, 1219–1221.

Kosarev, G., R. Kind, S. V. Sobolev, X. Yuan, W. Hanka, and S. Oreshin (1999), Seismic evidence for a detached Indian lithospheric mantle beneath Tibet, *Science*, *283*, 1306–1309.

Lehmann, I. (1961), *S* and the structure of the upper mantle, *Geophys. J. R. Astron. Soc.*, *4*, 124–138.

McNamara, D. E., W. R. Walter, T. J. Owens, and C. J. Ammon (1997), Upper mantle velocity structure beneath the Tibetan plateau from *Pn* travel time tomography, *J. Geophys. Res.*, *102*(B1), 493–505.

Meissner, R., F. Tilmann, and S. Haines (2004), About the lithospheric structure of central Tibet based on seismic data from the Indepth III profile, *Tectonophysics*, *380*, 1–25.

Nelson, K. D., et al. (1996), Partially molten middle crust beneath southern Tibet: Synthesis of project INDEPTH results, *Science*, *274*, 1684–1687.

Owens, T. J., and G. Zandt (1997), Implication of crustal property variations for models of Tibetan plateau evolution, *Nature*, *387*, 37–43.

Owens, T. J., G. E. Randall, F. T. Wu, and R. S. Zeng (1993), PASSCAL' instrument performance during the Tibetan plateau passive seismic experiment, *Bull. Seismol. Soc. Am.*, *83*, 1959–1970.

Revenaugh, J., and S. A. Sipkin (1994), Mantle discontinuity structure beneath China, *J. Geophys. Res.*, *99*, 21,911–21,927.

Shi, D., et al. (2004), Detection of southward intracontinental subduction of Tibetan lithosphere along the Bangong-Nuijang suture by *P*-to-*S* converted waves, *Geology*, *32*(3), 209–212.

Tapponnier, P., et al. (2001), Oblique stepwise rise and growth of the Tibet plateau, *Science*, *294*, 1671–1677.

Vergne, J., et al. (2002), Seismic evidences for stepwise thickening of the crust across the NE Tibetan plateau, *Earth Planet. Sci. Lett.*, *302*, 25–33.

Wenbo, W., et al. (2001), Detection of widespread fluids in the Tibetan crust by magnetotelluric studies, *Science*, *292*, 716–718.

Wittlinger, G., et al. (2004), Teleseismic imaging of subducting lithosphere and Moho offsets beneath western Tibet, *Earth Planet. Sci. Lett.*, *221*, 117–130.

Zhao, W., K. D. Nelson, and INDEPTH Team (1993), Deep seismic reflection evidence for continental underthrusting beneath southern Tibet, *Nature*, *366*, 557–559.

Zhao, W., et al. (2001), Crustal structure of central Tibet as derived from project INDEPTH wide-angle seismic data, *Geophys. J. Int.*, *145*, 486–498.

V. Farra, Département de Sismologie, Institut de Physique du Globe Paris, case 89, 4 Place Jussieu, F-75252 Paris Cedex 05, France. (farra@ipgp.jussieu.fr)

J. Vergne, Laboratoire de Géologie, Ecole Normale Supérieure, 24 rue Lhomond, F-75231 Paris Cedex 05, France. (vergne@geologie.ens.fr)

G. Wittlinger, Ecole et Observatoire des Sciences de la Terre, 5 rue René Descartes, F-67084 Strasbourg Cedex, France. (gerard.wittlinger@eost.u-strasbg.fr)